Blackbody Emission from Laser Breakdown in High-Pressure Gases

A. Bataller,* G. R. Plateau, B. Kappus, and S. Putterman
Department of Physics and Astronomy, University of California, Los Angeles, Los Angeles, California 90095, USA
(Received 14 April 2014; published 15 August 2014)

Laser induced breakdown of pressurized gases is used to generate plasmas under conditions where the atomic density and temperature are similar to those found in sonoluminescing bubbles. Calibrated streak spectroscopy reveals that a blackbody persists well after the exciting femtosecond laser pulse has turned off. Deviation from Saha's equation of state and an accompanying large reduction in ionization potential are observed at unexpectedly low atomic densities—in parallel with sonoluminescence. In laser breakdown, energy input proceeds via excitation of electrons whereas in sonoluminescence it is initiated via the atoms. The similar responses indicate that these systems are revealing the thermodynamics and transport of a strongly coupled plasma.

DOI: 10.1103/PhysRevLett.113.075001 PACS numbers: 52.50.Jm, 52.20.−j, 52.27.Gr, 78.60.Mq

The passage of a sound wave through a fluid can lead to pulsations of a gas bubble that are so strong that a dense plasma forms at its minimum radius. The degree of ionization $n_e \sim 10^{21}$ cm^{-3} is much larger than follows from Saha's equation at the measured temperature $T \sim 10\,000$ K. Experiments on sonoluminescence (SL) have been interpreted in terms of screening and correlations which modify the equation of state at atomic densities that are over an order of magnitude lower than expected from theories of strongly coupled plasma (SCP) [1–8]. The SL microplasma is created via direct heating of the atoms. Mechanical energy from the sound field sets up an implosion that compresses and heats the atoms to the point where they ionize. The liberated electrons are brought up to the ion or atom temperature via collisions. The emitted thermal spectrum is mainly due to collisions of hot electrons with ions. In low frequency (~40 Hz) experiments the flash width is hundreds of nanoseconds and the electron temperature is in local thermodynamic equilibrium (LTE) with the ions and light. If the unexpected high ionization and resulting opacity of a sonoluminescing bubble is due to fundamental changes in the equation of state of SCPs, then these effects should be independent of the path by which the temperature and density are reached. To test whether the SL microplasma is a manifestation of a new thermodynamic state, we have generated similar plasmas using laser breakdown in high-pressure gases with atomic densities between 10^{19}–10^{21} cm^{-3}, which reaches the density of SL in acids [2,5,6,9]. In this case, the path for energy flow is the reverse of SL as femtosecond laser pulses instantly ionize and energize the electrons while the ions remain cold. We report observation of an opaque plasma that persists well after the laser has turned off, and for times much longer than the recombination time scale. The plasma properties are consistent with the equations of state of the SL microplasmas and temporal evolution of the blackbody temperature provides insights into transport in SCPs.

The focusing of high-intensity laser pulses into gaseous media begins with a rapid ionization and heating of electrons. This is followed by a plasma expansion into the surrounding gas, whose luminous front vs time is shown in Fig. 1. The microplasma in Fig. 1 was generated using a 120 fs Ti:sapphire laser (Spectra-Physics) operating at 1 kHz with an adjustable energy of 0–1 mJ/pulse. The laser was focused with a 6 cm lens into the center of a pressure chamber. Optical access through the chamber was provided by fused silica viewports (Rayotek). The plasma's

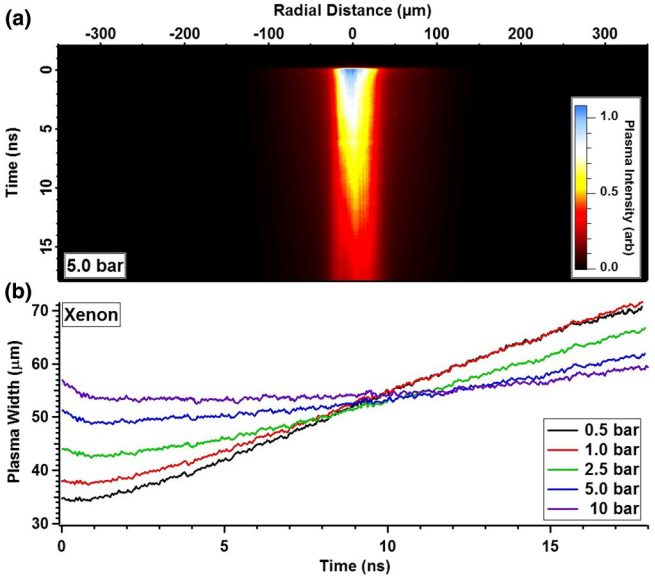

FIG. 1 (color online). Spectrally integrated plasma emission (> 495 nm) vs radius and time. The streaked image (a) was acquired for 5 bar xenon breakdown using a laser energy of 235 ± 4 μJ/pulse, where $t = 0$ indicates the moment of laser breakdown. The plasma's waist (FWHM) is plotted vs time (b) for various pressures. Plasma expansion becomes hindered with increasing pressure until ~5 bar is reached, at which point the plasma waist dwells before expanding.

light emission was collected and imaged by a 90 mm UV-to-near-infrared triplet lens (Edmund Optics). The plasma image was magnified by 5.34 and imaged onto the entrance slits of a 150 mm Czerny-Turner spectrometer (Princeton Instruments). The spectrally resolved plasma image was temporally resolved by aligning the spectrometer's output onto the entrance slits of a streak camera (Hamamatsu). The streak image in Fig. 1(a) is produced by keeping the spectrometer's entrance slits fully open (3 mm) and moving the grating to 0th order. Similarly, the spectral images in Fig. 2 were acquired by closing down the spectrometer's entrance slits (30 μm) and moving the grating to 1st order. The total amount of incident light entering the system in either mode is defined by the overlapping slit areas. The plasma image could be moved relative to the imaging system allowing spectral analysis at any plasma location. The spectral measurements presented in this Letter contain light from a plasma area of 32 μm^2 and was located at the center of the plasma column.

Because of the limited amount of light entering the imaging system, each spectral image (Fig. 2) consisted of an average of 6×10^5 breakdown events. However, shot-to-shot plasma intensity fluctuated by only ~10% and optical triggering resulted in a minimal temporal jitter of 20 ps. Both streak and spectral images show the plasma emission as a function of time, where $t_0 = 0$ ns marks the moment of laser breakdown. Indeed, laser-plasma scattering can enter the imaging system at the moment of breakdown and provide both a breakdown time stamp and a measurement for the system's temporal resolution. An example of this is present in Fig. 2(a) for t_0 and at the laser wavelength of 825 nm.

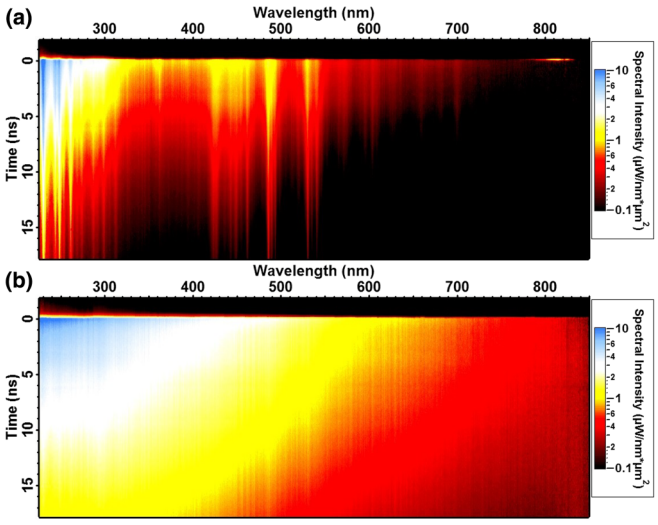

FIG. 2 (color online). Calibrated spectrum vs time for xenon breakdown at (a) 0.5 and (b) 5 bar using a laser energy of 235 ± 4 μJ/pulse. At lower pressures, the plasma spectrum is dominated by atomic line emission. With increasing pressure, the spectrum is broadened until it becomes completely continuous (~5 bar).

A plasma's absolute spectral intensity provides important information regarding its opacity and mechanism of light emission. For this purpose, the imaging system was calibrated against known sources (deuterium and quartz tungsten halogen lamps) and corrected for solid angle. A temporal correction (< 30 ps) was made to account for chromatic dispersion within the imaging optics. Finally, an intensity correction was applied due to chromatic aberration and tested against the known sources.

Spectral images were measured as a function of static pressure p_0 for xenon, argon, and helium while maintaining a fixed laser power. For low p_0 [Fig. 2(a)], the plasma spectrum is dominated by atomic lines for all times recorded. As p_0 is increased, the continuum radiation rises while the atomic lines become heavily broadened. This trend continues until a critical pressure p_c is reached, where the spectrum becomes completely continuous for early times [Fig. 2(b)], which has been observed in a similar system [10]. The gas-dependent value of p_c is ~5, 20, and 60 bar for xenon, argon, and helium, respectively. The continuous nature at p_c is visualized in Fig. 3, where individual spectra are extracted from Fig. 2(b) and plotted vs wavelength. For $p_0 = p_c$, continuous emission persists for a characteristic time scale t_{line}. This time scale is also gas dependent and is approximately 5, 1.5, and 0.15 ns for xenon, argon, and helium, respectively. For $t > t_{\text{line}}$, line emission emerges from the continuum and grows in strength relative to the continuum. This effect is observed in Fig. 3 for the Xe I transition line at 823 nm.

In the field of SL and SCP, testing spectra for opacity has proven to be a powerful technique for uncovering plasma properties [2,5–7,11–13]. The spectral intensity radiated by an ideal blackbody at temperature T is

$$I_\lambda = \frac{2\pi hc^2}{\lambda^5(\exp\{\frac{hc}{\lambda k_B T}\} - 1)}. \quad (1)$$

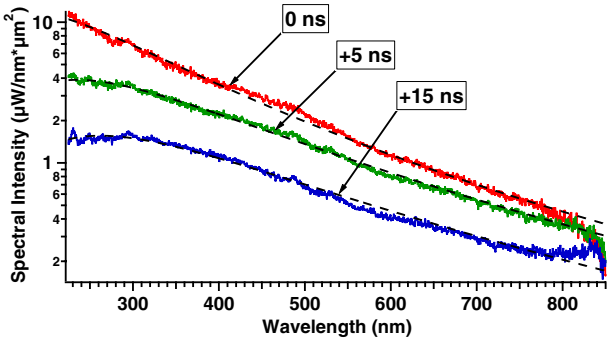

FIG. 3 (color online). Spectral intensity for 5 bar xenon breakdown at different times relative to the plasma formation. Blackbody fits (dashed curves) are plotted for each spectrum with values of $T = 16\,350$, $12\,350$, and $11\,050$ K for $t = 0$, +5, and +15 ns, respectively.

Deviation from blackbody behavior is quantified by multiplying I_λ by an effective emissivity ϵ, where $\epsilon = 1$ represents an ideal blackbody. Blackbody curves are presented in Fig. 3 and are well fit to the spectra. Fits were performed using a standard iterative method that minimizes the value of χ^2. T and ϵ from the blackbody fits are plotted vs time in Fig. 4(a). High opacity is observed as $\epsilon > 0.8$ for $t < 14$ ns and approaches $\epsilon \approx 1$ at $t \approx 5$ ns. Consistent with the definition of a blackbody as the ideal radiator at a given temperature, the emissivity in Fig. 4(a) never grows above unity (within experimental error ~15%) even though the plasma temperature is decreasing exponentially. Further blackbody behavior is observed by measuring the emissivity value of the opaque 823 nm Xe I transition line ϵ_{823}. Using the blackbody temperature, the intensity at 823 nm, and Eq. (1), ϵ_{823} is plotted vs time in Fig. 4(a). For $t > t_{\text{line}}$, the plasma becomes increasingly transparent as indicated by the reduced emissivity and increased atomic line contribution to the spectrum. However, the emissivity for the strong 823 nm line remains opaque ($\epsilon_{823} \approx 1$) for $t > t_{\text{line}}$. Like ϵ, ϵ_{823} is never greater than unity, which has been observed in other blackbody plasmas [2]. High opacity is also observed for 25 bar argon and 74 bar helium in Figs. 4(b) and 4(c), respectively. With the exception of 5 bar xenon, ϵ begins near unity and drops after a time corresponding to the end of the exponential temperature decay. Possible reasons for the initial growth in ϵ for xenon breakdown are an increasing electron density after breakdown (as observed in [10]) and a plasma temperature gradient producing a near-blackbody spectrum.

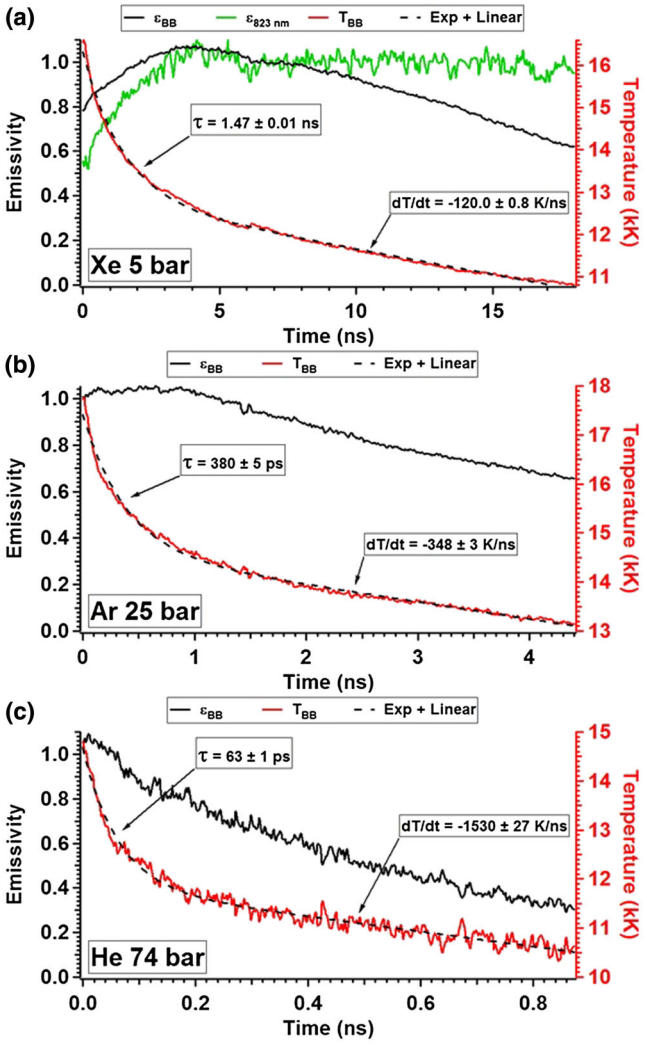

FIG. 4 (color online). Blackbody temperature (red curve) and effective emissivity (black curve) as a function of time for (a) 5 bar xenon, (b) 25 bar argon, and (c) 74 bar helium. Laser energies of 235 ± 4, 325 ± 3, and 570 ± 6 μJ/pulse were used for xenon, argon, and helium, respectively. For all gases, the temperature initially decays exponentially and is followed by a long linear decay. A fit to an exponential plus linear function is plotted (dashed curve) for each gas with characteristic time scales indicated. For xenon, the emissivity for the opaque Xe I transition is plotted (green curve) using the spectral intensity at 823 nm and the blackbody temperature.

When the observed opacity is interpreted in terms of transport theory in SCPs, an estimate of the charge density can be obtained. A key condition for opacity is that the photon mean free path is smaller than the radiating body, written as $\kappa R > 1$, where R is the plasma thickness and κ is the absorption coefficient of light. For dense plasma, the dominant form of absorption is the process of free-free inverse bremsstrahlung where an electron absorbs light during a "collision" with an ion [14]. The collisionality in SCP is greatly affected by collective screening effects. In the presence of an oscillating electromagnetic field of frequency ω, the collisionality is characterized by the unitless parameter $\omega\tau_\omega$, where τ_ω is the collision time of an electron with an ion. For an SCP in the multi-ionization regime [7]

$$\omega\tau_\omega = \left[\frac{2}{\sqrt{6\pi}}\gamma^{1/2}\Gamma^{1/2}\Gamma_\omega \ln\left(\frac{0.7}{\sqrt{3}}\Gamma_\omega^{-3/2} + 1\right)\right]^{-1}, \quad (2)$$

where γ is a unitless parameter representing the plasma frequency, Γ is the plasma coupling parameter, and Γ_ω is the plasma coupling parameter in the presence of an electromagnetic field. These quantities are given by

$$\gamma = \left(\frac{\omega_p}{\omega}\right)^2 = \frac{4\pi n_0 \bar{Z} e^2}{m_e \omega^2}, \qquad \Gamma = \left(\frac{\bar{Z}e^2}{k_B T}\right)\left(\frac{4\pi n_0}{3}\right)^{1/3},$$

$$\Gamma_\omega = \Gamma\left[\frac{k_B T}{\hbar\omega}\left(1 - \exp\left(-\frac{\hbar\omega}{k_B T}\right)\right)\right],$$

where $\bar{Z} = n_e/n_0$ is the effective ionization level, $n_0(n_e)$ is the nuclei(electron) density, and m_e is the electron mass. For $\bar{Z} < 1$, $\Gamma = (e^2/k_B T)(4\pi\bar{Z}n_0/3)^{1/3}$. The Coulomb logarithm in Eq. (2) represents screening effects and was

found using a molecular dynamics simulation [15] and later supported in a laser-SL coupling experiment [7]. In the plasma regime where $\gamma \ll 1 \ll \omega\tau_\omega$, the absorption coefficient reduces to $\kappa = (\omega/c)(\gamma/\omega\tau_\omega)$. For 5 bar xenon breakdown at $t = 5$ ns, $T = 12\,350$ K, $n_0 = 1.25 \times 10^{20}$ cm^{-3}, $R = 50$ μm [Fig. 1(b)], and selecting a spectral region relatively void of strong line emission (400 nm), an electron density of $n_e > 4.0 \times 10^{20}$ cm^{-3} is needed to satisfy the observed opacity ($\kappa R \approx \pi$). This electron density requires over 3 levels of ionization and results in an SCP with $\Gamma > 3.5$. The initial attainment of such high levels of ionization is well known [16,17]. We find that this level persists for an extended time and is a property of the equation of state of SCP.

The temporal evolution of the opaque spectrum yields the temperature as a function of time when $\epsilon \approx 1$ (Fig. 4). This behavior can be connected to the transport in SCP, in particular, the electron-ion collision time

$$\tau_{e-i} = \lim_{\hbar\omega\to 0} \tau_\omega = \left[\frac{2}{\sqrt{6\pi}}\omega_p \Gamma^{3/2} \ln\left(\frac{0.7}{\sqrt{3}}\Gamma^{-3/2} + 1\right)\right]^{-1}. \tag{3}$$

This is the time scale for electron-ion energy transfer and follows from Eq. (2) in the limit of no electric field. We argue that τ_{e-i} accounts for the initial exponential drop in temperature soon after the laser-gas interaction. The intense laser pulse forms a plasma in the pressurized gas via the process of multiphoton ionization [18]. Recombination rapidly brings the electron density and light emission into LTE at the measured spectral temperature while leaving the ions cold. Because of their large mass, the ions take a longer time to heat up via collisions with the energetic electrons in a time scale $\tau_{\rm th} \approx (M/m_e)\tau_{e-i}$, where M is the ion mass [14]. As the ions heat up, the electron temperature drops exponentially (Fig. 4). Opacity as deduced from the blackbody spectrum only yields a lower bound on the plasma density. However, this bound becomes the actual electron density for plasmas transitioning from opaque to transparent spectrum. This is the point at which ϵ first drops below 1. This also corresponds to the end of the exponential temperature decay at $t \approx 5/1/0.1$ ns for 5/25/74 bar Xe/Ar/He breakdown [Figs. 4(a), 4(b), 4(c)]. Using $T = 12\,350/14\,550/12\,550$ K, $R = 50/37/25$ μm, $n_e = 4.0/6.3/7.0 \times 10^{20}$ cm^{-3} (required for opacity at 400 nm), and Eq. (3) the calculated thermalization time is 1170/305/28 ps. For the range of Γ given above, Eq. (3) can be approximated as $\omega_p\tau_{e-i} \approx 5.37$ matching [15]. Therefore, the theory of $\tau_{\rm th}$ in this regime is approximately temperature-independent and can be reasonably approximated using plasma values at the end of the exponential decay. This allows us to extrapolate the exponential behavior to the initial temperature decay and obtain the best fit values of 1470/380/63 ps. Comparison of all gases results in a $\tau_{\rm th}$ that is roughly linear to the ion mass. Normalizing to argon, the ratio of atomic masses is 3.3:1:0.10 (Xe:Ar:He). Similarly, the ratio of the measured decay time divided by τ_{e-i} is 3.3:1:0.13, which is consistent with the screened theory of collisions in SCP as applied via Eq. (3) [15]. Had we used the collision time appropriate to dilute plasma theory we would have found $\tau_{\rm th} = 160/71/5.2$ ps.

Although rapid ionization from high-intensity laser pulses has been achieved in a variety of systems [10,19–21], we further observe that high ionization is maintained for a surprisingly long period of time. Is the persistent electron density due to local electronic thermodynamic equilibrium or far off-equilibrium behavior due to a long recombination time? In other words, is the plasma in ionization equilibrium at each time step in Fig. 4? To address this question, we consider the three-body recombination time scale $\tau_{\rm rec}$ from plasma theory (photorecombination plays a minor role [14]) which occurs from the capture of an electron by an ion in the presence of an additional electron, given by

$$\tau_{\rm rec} = (\bar{v_e}\pi^2 r_0^5 \bar{Z}^4 n_0^2)^{-1}, \tag{4}$$

where $\bar{v_e} = \sqrt{8k_BT/m_e\pi}$ is the mean thermal electron speed and $r_0 = 2e^2/3k_BT$ is the impact parameter for recombination in a Coulomb collision. Equation (4) and the plasma properties for xenon at $t = 5$ ns results in an impossibly fast recombination time of 0.15 fs. This is a result of dilute plasma theory applied to the dense plasma which we study. In formulating Eq. (4), screening processes are not accounted for and will result in an overestimation of the probability of finding a second electron in the vicinity of the electron-ion collision. To this end, we account for screening by replacing r_0 with the screened impact parameter ρ given by $\sigma = \pi\rho^2 = (\bar{Z}n_0\bar{v_e}\tau_{e-i})^{-1}$. The result of this substitution is that every electron-ion collision can result in a recapturing of the electron, and, therefore, $\tau_{\rm rec} \approx \tau_{e-i}$. This time scale is still much faster than any experimental time scale and is necessarily smaller than $\tau_{\rm th}$. We conclude the ionization is in a state of LTE with the electron temperature and light emission.

Ionization for an electron plasma in LTE is governed by Saha's equation given as

$$\frac{x_{m+1}x_e}{x_m} = \frac{2}{n_0}\frac{u_{m+1}}{u_m}\left(\frac{m_e k_B T}{2\pi\hbar^2}\right)^{3/2} \exp\left(-\frac{\chi_m}{k_B T}\right), \tag{5}$$

where $x_m(x_e)$, u_m, and χ_m is the ion(electron) concentration, electronic partition function, and ionization potential for the mth ion, respectively [14,22]. Although the electrons and ions are at different temperatures for $t < \tau_{\rm th}$, Eq. (5) still applies by using the electron temperature [23]. For 5 bar xenon at $t \approx 5$ ns, the charge density is $> 4 \times 10^{20}$ cm^{-3} while the temperature is only $\sim$12 000 K. According to Saha's equation, the degree of ionization

for the first ionization level ($m = 0$ and $\chi_1 = 12.1$ eV) should be less than 3%. Yet the opacity suggested by our data requires over 3 levels of ionization. Therefore, the collective processes at work in SCP must reduce the overall ionization potential by an amount comparable to χ_3. In particular, the lowering of χ_m through Debye screening results in a change of the average ionization potential by [14,22]

$$\bar{\Delta\chi} = 2(\bar{Z}+1)e^3\sqrt{\frac{\pi\bar{Z}(\bar{Z}+1)n_0}{k_BT}}. \quad (6)$$

Using the measured plasma properties of xenon breakdown ($\bar{Z} = 3.2$), the ionization potential is dramatically reduced by $\bar{\Delta\chi} = 32$ eV. This value of potential reduction, albeit remarkably high, is consistent with the observed level of ionization as it lies between $\chi_3 = 31.1$ and $\chi_4 = 41.0$ eV.

Application of calibrated streaked spectroscopy to femtosecond laser breakdown in high-pressure gases reveals both transport and thermodynamic properties of strongly coupled plasmas. We observe micron-scale blackbody spectra that persist long after the exciting laser has been turned off. Spectral analysis indicates the presence of a plasma with a higher ionization when compared to Saha's equation. We conclude a strongly coupled LTE plasma is formed in an unexpected region of parameter space (defined by atomic density and temperature). The time scale for thermal relaxation depends strongly on density effects and its measurement discriminates between various theories, selecting in favor of [15]. Future work will study the dwell time and expansion of the strongly coupled plasma. These systems may possibly reach regions of parameter space occupied by matter obeying quantum statistics. The discovery of an opaque microplasma as a thermodynamic state suggests electric discharges in pressurized gases as a new route toward optical switches.

We gratefully acknowledge support from DARPA MTO for research on microplasmas. We thank Brian Naranjo, Keith Weninger, Carlos Camara, Gary Williams, and John Koulakis for valuable discussions.

*bataller@physics.ucla.edu

[1] K. S. Suslick and D. J. Flannigan, Annu. Rev. Phys. Chem. **59**, 659 (2008).
[2] B. Kappus, S. Khalid, A. Chakravarty, and S. Putterman, Phys. Rev. Lett. **106**, 234302 (2011).
[3] B. Kappus, S. Khalid, and S. Putterman, Phys. Rev. E **83**, 056304 (2011).
[4] K. S. Suslick, N. C. Eddingsaas, D. J. Flannigan, S. D. Hopkins, and H. Xu, Ultrason. Sonochem. **18**, 842 (2011).
[5] S. Khalid, B. Kappus, K. Weninger, and S. Putterman, Phys. Rev. Lett. **108**, 104302 (2012).
[6] B. Kappus, A. Bataller, and S. J. Putterman, Phys. Rev. Lett. **111**, 234301 (2013).
[7] A. Bataller, B. Kappus, C. Camara, and S. Putterman, Phys. Rev. Lett. **113**, 024301 (2014).
[8] D. J. Flannigan and K. S. Suslick, Nat. Phys. **6**, 598 (2010).
[9] S. Hopkins, S. Putterman, B. Kappus, K. Suslick, and C. Camara, Phys. Rev. Lett. **95**, 254301 (2005).
[10] S. V. Garnov, V. V. Bukin, A. A. Malyutin, V. V. Strelkov, P. R. Bolton, H. Daido, and S. V. Bulanov, AIP Conf. Proc. **1153**, 37 (2009).
[11] O. Baghdassarian, B. Tabbert, and G. A. Williams, Phys. Rev. E **75**, 066305 (2007).
[12] M. Skowronek, J. Rous, A. Goldstein, and F. Cabannes, Phys. Fluids **13**, 378 (1970).
[13] Y. Vitel and M. Skowronek, J. Phys. B **20**, 6477 (1987).
[14] Y. P. Zel'dovich and Ya. B. Raizer, *Physics of Shock Waves and High-Temperature Hydrodynamic Phenomena* (Dover, New York, 1966), ISBN 0-486-42002-7.
[15] G. Dimonte and J. Daligault, Phys. Rev. Lett. **101**, 135001 (2008).
[16] W. M. Wood, C. W. Siders, and M. C. Downer, Phys. Rev. Lett. **67**, 3523 (1991).
[17] B. M. Penetrante, J. N. Bardsley, W. M. Wood, C. W. Siders, and M. C. Downer, J. Opt. Soc. Am. B **9**, 2032 (1992).
[18] J. Noack and A. Vogel, IEEE J. Quantum Electron. **35**, 1156 (1999).
[19] N. Bloembergen, IEEE J. Quantum Electron. **10**, 375 (1974).
[20] T. Ditmire, J. W. G. Tisch, E. Springate, M. B. Mason, N. Hay, R. A. Smith, J. Marangos, and M. H. R. Hutchinson, Nature (London) **386**, 54 (1997).
[21] F. Quéré, S. Guizard, and P. Martin, Europhys. Lett. **56**, 138 (2001).
[22] H. R. Griem, Phys. Rev. **128**, 997 (1962).
[23] X. Chen and P. Han, J. Phys. D **32**, 1711 (1999).